A Comprehensive Method of Ambiguity Suppression for Constellation of Geostationary and Low Earth Orbit SAR

Peng Xiao, *Member, IEEE*, Wei Guo, Youming Wu, and Bo Liu

***Abstract*—ConGalSAR is a novel SAR constellation that has an outstanding performance of revisit and economy. In the system, with the MirrorSAR technology, one geostationary illuminator and several economical low earth orbit transponders work together to achieve a short revisiting interval. Because of the huge difference in the distances of transmitting and receiving, the spatial weighting of the antenna patterns on the ground is quite different, which leads to the deterioration of ambiguity to signal ratio. The multiphase center and digital beamforming antennas can suppress the ambiguity energy; however, they are too expensive and heavy to be equipped on the dozens of transponding nanosatellites. In this article, a comprehensive ambiguity suppression method, including the reflector antenna design and signal processing, is proposed to reduce the ambiguity ratio, which well solves the ambiguity problem under the condition of the low manufacturing costs and lightweight transponders. In terms of the hardware design, the multifeed reflector antenna is applied to the transponder, in which the feeds receive an echo together. Based on this, the low sidelobes beamforming is achieved to well suppress the ambiguity. Meanwhile, the amplitude-modulated chirps are also used here aiming at the residual ambiguity in the large dynamic scene. Through spectral selection and extrapolation processing, range ambiguity energy is suppressed more while preserving the resolution. The digital simulations show that the comprehensive method can realize −20 dB ambiguity ratios at least, which conforms to the ambiguity-to-signal ratio design of ConGaLSAR.**

***Index Terms*—Ambiguity suppression, bistatic SAR (BiSAR), multifeed reflector antenna, spectral selection and extrapolation, synthetic aperture radar (SAR).**

I. Introduction

CONGALSAR is a novel short revisiting multistatic synthetic aperture radar (SAR) system, which contains one geostationary illuminator and dozens of low earth orbit (LEO) transponders [1]. With MirrorSAR technology [2]–[4], ConGaLSAR gives an economical way to construct a constellation with a 3-m resolution and 72-min averaging revisiting interval while ensuring time and frequency synchronizations.

Because of the huge difference in the distances of transmitting and receiving, the spatial weighting of the antenna patterns projected on the ground is also different, which leads to the deterioration of the ambiguity to signal ratio (ASR) [including azimuth ambiguity to signal ratio (AASR) and range ambiguity to signal ratio (RASR)]. In the classic SAR system design [5], these two factors restrict each other, which influences the improvement of the azimuth resolution and range swath width.

Alternating orthogonal transmitting signals are often used to resolve the range ambiguity problem [6]–[8]. Although the ambiguity echo is not focused along with the range after pulse compression, the ambiguity energy still remains in the image. Thus, the orthogonal transmitting signals with the same carrier frequency provide limited help to the range ambiguity suppression, especially for weak targets detection [9]. The existing azimuth ambiguity suppression methods for the SAR images mainly rely on the notably different Doppler weighting caused by azimuth antenna patterns [11]–[13]. However, in ConGaLSAR, the illuminating pattern is much wider than the receiving one; thus, the Doppler weighting differentiation goes worse, leading to the invalidation of the algorithms above. Moreover, the multichannel antenna technology, such as multiantenna phases or digital beamforming, is an effective way to suppress the ambiguity energies [14]–[17] but at the huge expense of system complexity, antenna weight, and manufacturing cost, which is obviously not suitable for the design of the transponders in ConGaLSAR. Besides, some challenges for the multichannel technology still exist, such as the equivalent phase-center errors among the receiving channels responsible for a series of false targets, which are difficult to be removed completely [15], [18], [19], as well as the pulse extension loss.

In this article, a comprehensive method, including reflector antenna design and signal processing, is proposed to solve the ambiguity problem in the ConGaLSAR system. The former reduces the antenna pattern sidelobes on the transponder in hardware, and the latter mathematically suppresses the ambiguity energy of strong scattering targets more.

A multifeed reflector antenna achieves the electronic beam steering capability by directing the power to different feeds

Manuscript received February 19, 2020; revised May 19, 2020 and June 1, 2020; accepted June 10, 2020. Date of publication June 15, 2020; date of current version June 29, 2020. This work was supported in part by the Innovation Workstation of Qian Xuesen Lab and in part by the Innovation Project of CAST. *(Corresponding author: Wei Guo.)*

Peng Xiao and Bo Liu are with the Qian Xuesen Laboratory of Space Technology, China Academy of Space Technology, Beijing 100094, China (e-mail: xiaopeng@qxslab.cn; liubo@qxslab.cn).

Wei Guo is with the Department of Land Surveying and Geo-Informatics, The Hong Kong Polytechnic University, Hong Kong (e-mail: guowei19900331@163.com).

Youming Wu is with the Aerospace Information Research Institute, Chinese Academy of Sciences, Beijing 100190, China, and also with the Key Laboratory of Network Information System Technology (NIST), Aerospace Information Research Institute, Chinese Academy of Sciences, Beijing 100190, China (e-mail: youming_wu@yeah.net).

Digital Object Identifier 10.1109/JSTARS.2020.3002392

[21]. This kind of lightweight and simple structure antenna has been used in the minisatellite (e.g., TecSAR [23]) or long wavelength system (e.g., Tandem-L [24]). In ConGaLSAR, the feeds will receive an echo together but not independently, which realizes a weighted beam between the reflector and feed array acquiring the lower sidelobes of the antenna pattern. In addition, the broadening main lobe extends the range swath and enhances the azimuth resolution with a bigger reflector diameter.

For the special scene, particularly the large dynamic areas, such as the coast, the range ambiguity still appears in the final image despite applying the multifeed reflector antenna. In this article, a resolution preserving range ambiguity suppression algorithm based on the amplitude-modulated chirps is proposed to suppress the residual range ambiguity more. The amplitude-modulated chirps are transmitted alternately, which leads to the amplitude difference in the range spectrum. By the bandpass filter, the ambiguity suppression is realized but with the degradation of the spatial resolution. A spectral extrapolation proposed in [26] is used to recover the information from the cutoff frequency. This method has better robustness compared with the other algorithms, for the energy distribution in the original image is used to establish accurate prior information.

With the digital simulations and real data experiments, it is shown that the AASR and RASR can be suppressed to less than −20 dB by the multifeed reflector antenna and the range ambiguity energy of the strong scattering targets can be suppressed more than 4.7 dB more by the mathematical processing.

The rest of this article is organized as follows. In Section II, the ConGaLSAR system is briefly introduced and the special ambiguity problem is also analyzed. In Section III, the design of the multifeed reflector antenna is presented to suppress the ambiguity. Section IV introduces the range ambiguity suppression algorithm based on the amplitude-modulated chirp signals. The ambiguity suppression performance of the comprehensive method is analyzed through simulations in Section V. Section VI concludes the article.

II. Ambiguity of ConGaLSAR

A. System Description

In order to solve the time and phase synchronizations for bistatic SAR (BiSAR) and further reduce the system cost, a novel transponding mode modified from MirrorSAR is adopted in ConGaLSAR. Specifically, as shown in Fig. 1, the chirp signal is first transmitted from the geostationary orbit satellite and illuminates a wide area. Then, the echo is received by the LEO satellite, which is designed as an analog signal transponder. Different from common BiSAR, the echo is modulated to a higher frequency and finally retransmitted back to the illuminator for sampling.

The typical system parameters of ConGaLSAR are given in Table I. As discussed in [1], the azimuth resolution of the stripmap mode is approximately equal to the diameter of the receiving antenna on the transponder with an effective azimuth bandwidth of about 2800 Hz. Because the transmitter and receiver do not use the same antenna hardware, the transmitting

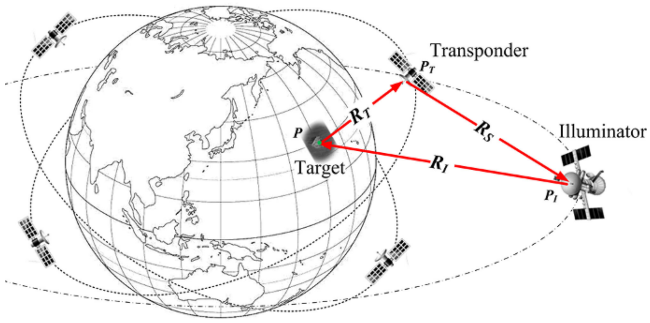

Fig. 1. Geometry of the ConGaLSAR system.

TABLE I
System Parameters of ConGaLSAR

Parameter	Symbol	Value
Illuminator altitude	H_I	35786 km (stationary)
Transponder altitude	H_T	400 km
Wavelength	λ	0.03 m
Illuminator antenna size	A_I	300 m^2 (20 m dia. dish)
Transponder antenna size	A_T	7 m^2 (3 m dia. dish)
Satellite link wavelength	λ_T	0.01 m
Satellite link antenna size	A_c	3 m^2
Amplification factor	M	110 dB
Maximum bandwidth	B_r	300 MHz
Ground resolution	ρ_r	3 m
Azimuth resolution	ρ_a	3 m
Average transmit power	P_{ave}	2000 W
Integration time	T_a	0.5-1 s (variable)
Noise figure & losses	$F_T + L$	5 dB
Ambiguity to signal ratio	ASR	≤-20 dB
Noise-equivalent sigma zero	$NESZ$	≤-20 dB

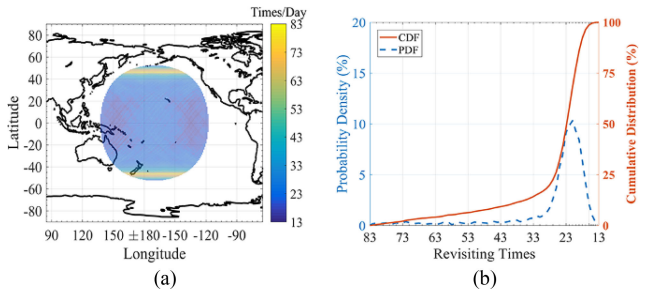

Fig. 2. Effective observing area of ConGaLSAR. (a) Revisiting times in one day. (b) Statistical distribution of the revisiting times for the effective observing area in one day.

pulse occlusion is unnecessary to be considered. Therefore, the choice of the pulse repetition frequency (PRF) will be more flexible. In a practical application, the illuminator is set to −170° longitude to light up the Pacific area. There are 24 transponder satellites with the equal interval right ascension of ascending nodes of 14°, which can realize the complete coverage of the earth between ±52° latitude averaging 20 times during one day, as shown in Fig. 2.

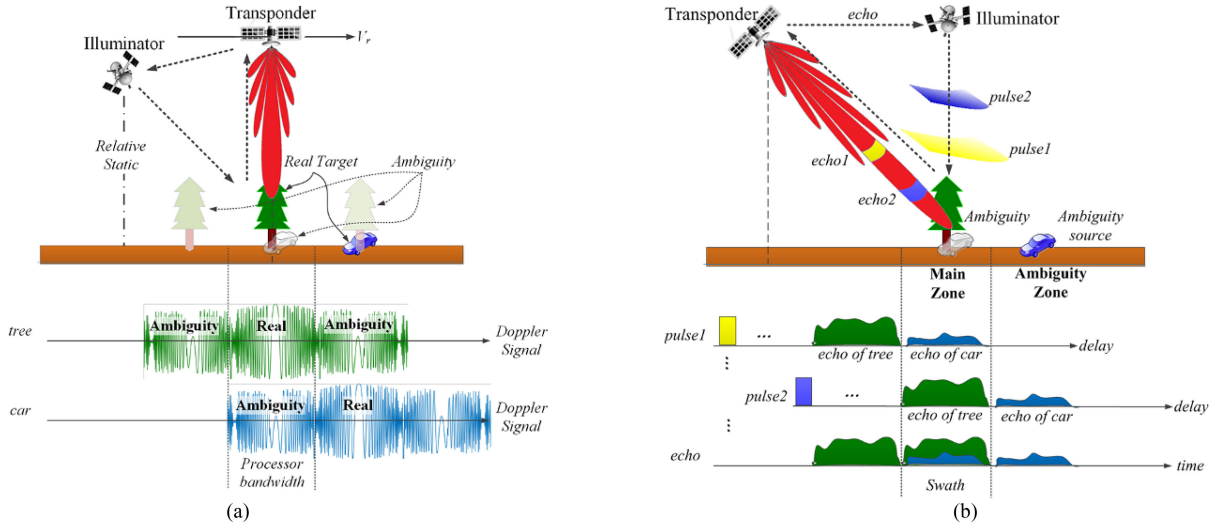

Fig. 3. Schematic diagram of ambiguity. (a) Azimuth ambiguity. (b) Range ambiguity.

B. Ambiguity

Generally, the effective azimuth bandwidth and range swath are determined by the half-power beamwidth. However, in the real situation, the antenna pattern is unlimited, thus the coverage of the beam involves quite a larger area actually. So, the root cause of the ambiguity is the gaps between the real antenna pattern and processing windows. For the SAR signal is separated to range and azimuth, the ambiguity should be analyzed respectively.

The azimuth ambiguity is caused by the sub-Nyquist sampling. In the real SAR system, the Doppler signal is weighted by the azimuth antenna pattern, whose half-power bandwidth is the effective azimuth bandwidth, which is used as a reference for the PRF design. However, the actual bandwidth of the Doppler signal is much more than PRF, which leads to the spectrum aliasing in the frequency domain corresponding to the ambiguity. Thus, the ambiguity targets will cover the real target, which shares the same spectrum regions [as shown in Fig. 3(a)].

Nevertheless, the range ambiguity derives from a different reason: the echo from the far object that is illuminated by the previous pulse overlaps with the echo from the near object in the next pulse [as shown in Fig. 3(b)]. The position of the false target is related to the PRF.

Traditionally, AASR and RASR are used to describe the influence of the ambiguity. Referring to the classic radar equation [5], the BiSAR signal-to-noise ratio (SNR) is

$$\mathrm{SNR} = \frac{\rho_r P_{\mathrm{avg}}}{\mathrm{PRF} \times D_R k T L F_r} \left(\frac{\lambda}{4\pi}\right)^3 \sigma_0 \frac{G_I G_R}{R_I^2 R_R} \tag{1}$$

where ρ_r is the ground resolution, P_{avg} is the average transmitting power, D_R is the diameter of the receiving antenna on the transponder, k is the Boltzmann constant, T is the system noise temperature, F_r and L are the noise figure and losses, respectively, λ is the carrier wavelength, σ_0 is the backscattering coefficient of the distributed target, G_I and G_R are the antenna gains of illuminating and receiving, respectively, and R_I and R_R are the distance from the target to the illuminator and the transponder, respectively.

Based on (1), AASR is defined as

$$\mathrm{AASR} = \frac{\sum\limits_{n\neq 0} \int_{n\times\mathrm{PRF}-B_a/2}^{n\times\mathrm{PRF}+B_a/2} G_I(f)\, G_R(f)\, df}{\int_{-B_a/2}^{B_a/2} G_I(f)\, G_R(f)\, df} \tag{2}$$

where f is the Doppler frequency, B_a is the effective Doppler bandwidth, and n is an integer. RASR is defined as

$$\mathrm{RASR} = \frac{\sum_{m\neq 0} \int_{-R/2+\Delta R_m^-}^{R/2+\Delta R_m^+} \left[G_I(r)\, G_R(r)\right] / \left[R_I^2(r)\, R_R(r)\right] dr}{\int_{-R/2}^{R/2} \left[G_I(r)\, G_R(r)\right] / \left[R_I^2(r)\, R_R(r)\right] dr} \tag{3}$$

where R is the range swath, r is the ground range from the target to the center of the scene, $R_I(r)$ and $R_R(r)$ are the distance from the target at r to the illuminator and the transponder, respectively, and m is an integer

$$\begin{aligned} &R_I\left(R/2+\Delta R_m^+\right) + R_R\left(R/2+\Delta R_m^+\right) \\ &\quad = R_I(R/2) + R_R(R/2) + c\times m/\mathrm{PRF} \end{aligned} \tag{4}$$

and

$$\begin{aligned} &R_I\left(-R/2+\Delta R_m^-\right) + R_R\left(-R/2+\Delta R_m^-\right) \\ &\quad = R_I(-R/2) + R_R(-R/2) - c\times m/\mathrm{PRF} \end{aligned} \tag{5}$$

where c is the light speed, ΔR_m^+ and ΔR_m^- are the range ambiguity distance from the farther zone and the nearer zone respectively, and $\Delta R_m^{\pm} = \pm c \times m/\mathrm{PRF}$.

Since the orbit radius of the illuminator is much bigger than the earth radius, the value range of $R_I(r)$ is less than 10%. Thus, (3) is simplified as

$$\mathrm{RASR} = \frac{\sum_{m\neq 0} \int_{-R/2+\Delta R_m^-}^{R/2+\Delta R_m^+} \left[G_I(r)\, G_R(r)\right] / R_R(r)\, dr}{\int_{-R/2}^{R/2} \left[G_I(r)\, G_R(r)\right] / R_R(r)\, dr}. \tag{6}$$

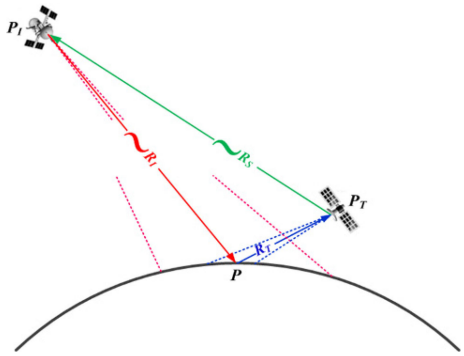

Fig. 4. Beam coverage of the illuminating and receiving antennas.

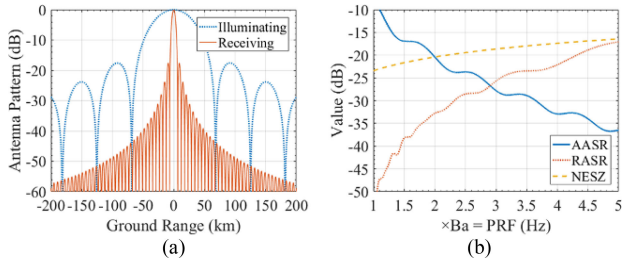

Fig. 5. Ambiguity of ConGaLSAR. (a) Different weighting of the antenna patterns on the ground. For the narrow receiving beam, the range swath is only 8 km. (b) Ambiguities and NESZ changing with PRF. When PRF is 2.9 × the effective azimuth bandwidth, ASR has the best balance point; however, NESZ deteriorates, which means the transmitting energy is wasted.

For the circular parabolic reflector antenna, the normalized pattern $G_0(\phi)$ depending on the spatial angle ϕ is approximated as [21]

$$G_0(\phi) = \frac{2J_1(\pi D \sin\phi/\lambda)}{\pi D \sin\phi/\lambda} \tag{7}$$

where D is the diameter of the antenna and J_1 is the one-order Bessel function.

It is clear that the rising of PRF can suppress AASR but make RASR and noise equivalent sigma zero (NESZ) worse, which is defined from (1) as

$$\text{NESZ} = \left(\frac{4\pi}{\lambda}\right)^3 \frac{D_R k T F_r L R_I^2 R_R}{\rho_r P_{\text{avg}} G_I G_R} \text{PRF}. \tag{8}$$

In the SAR systems, AASR, RASR, and NESZ are always set lower than -20 dB to ensure the image quality [5], [22], which is also used here as the standard of the system design for GonGaLSAR. Especially for the beam coverage shown in Fig. 4, although the beamwidth of the illuminating antenna is much smaller than the receiving one (due to a larger illuminating antenna size), the illuminating antenna pattern projected on the ground is much wider than the one of the latter, because of the huge distance difference. The different spatial weighting of the antenna patterns leads to worse ASR than the monostatic system and also wastes the illuminating energy.

For example, if the incidence angle of the illuminator and the emergence angle of the transponder are both 45°, which only leads to an 8 km range swath. The antenna patterns on the ground are shown in Fig. 5(a), and AASR, RASR, and the worst NESZ depending on PRF are shown in Fig. 5(b). From Fig. 5(b), when PRF is 2.9 times the effective azimuth bandwidth, ASR has the best balance point; however, NESZ deteriorates, which means the transmitting energy is wasted.

In conclusion, the narrow swath and poor system sensitivity limit the performance of ConGaLSAR; thus, it is necessary to reduce the redundancy in ASR and NESZ with economical methods.

III. Multifeed Reflector Antenna

Considering (2) and (6), it is obvious that the root cause of the ambiguity is derived from the antenna pattern. What is different is that the azimuth ambiguity is due to the nonbandlimited characteristic of the antenna pattern, while the range one is due to the unlimited swath characteristic. In order to eliminate the ambiguity from the source, a novel design of the multifeed reflector antenna is proposed in this section, which breaks the traditional ways of the ambiguity suppression through signal design and processing.

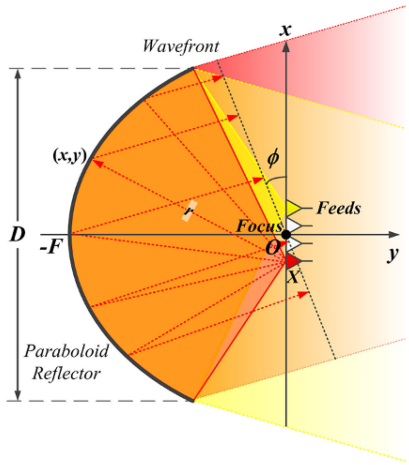

Fig. 6. Multibeam caused by the multifeed reflector antenna.

Nowadays, the reflector antenna has been widely used on the satellites owing to its lightweight, low cost, and high efficiency. As shown in Fig. 6, the multifeed reflector antenna achieves an electronic beam steering capability by directing the power to different feeds around the focus of the paraboloid.

The shape of the circle paraboloid reflector can be described as

$$y(x) = \left(x^2/4F\right) - F \text{ in which } |x| \le (D/2) \tag{9}$$

where F and D are the focal length and diameter of the reflector, respectively.

If the feed is moved X along the x-axis, the distance between the feed and any point (x, y) on the reflector is

$$\begin{aligned} r(x;X) &= \sqrt{y^2 + (x-X)^2} \\ &= \sqrt{(x^2/4F + F)^2 + X^2 - 2xX}. \end{aligned} \tag{10}$$

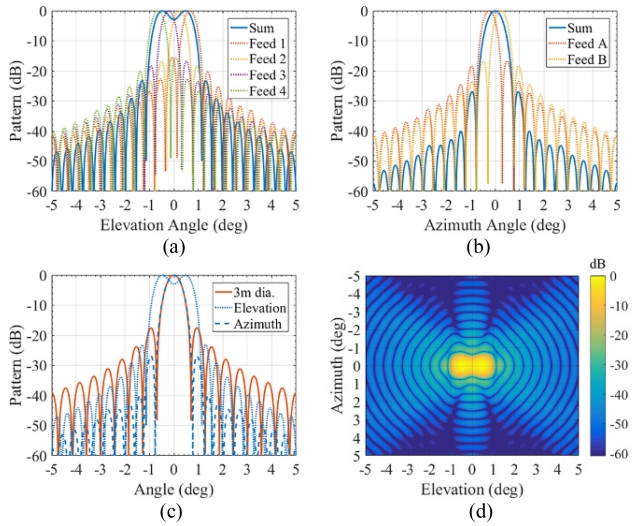

Fig. 7. Sum beam of the multifeed reflector antenna with 3.9 m dia., 2.48 m focal length, and 4 × 2 feeds. (a) Elevation slices. (b) Azimuth slices. (c) Sidelobes of the sum beam is much lower than the original one. The beamwidth in azimuth is similar to the original one and the beamwidth in the elevation is much wider, which achieves a bigger range swath. (d) 2-D pattern with the feed array.

With ray tracing [27], the electric field at direction angle ϕ is

$$E(\phi;X)=\int_{-D/2}^{D/2}\times\exp\left\{-j2\pi\frac{r(x;X)-y(x)\cos\phi-x\sin\phi}{\lambda}\right\}dx. \quad (11)$$

The displacement of the feed produces an odd-order phase error in the aperture, which causes an asymmetry of the sidelobes, and the beam will be steered by $\Delta\phi$ [27]

$$\Delta\phi(X)\approx\frac{X/F}{1+(X/F)^2}. \quad (12)$$

Based on this, if the feed array works together, the electric field at the direction angle ϕ is updated to

$$E(\phi)=\sum_{n=1}^{N}\int_{-D/2}^{D/2}\times\exp\left\{-j2\pi\frac{r(x;X_n)-y(x)\cos\phi-x\sin\phi}{\lambda}\right\}dx \quad (13)$$

where N is the total number of feeds, $n=1,2,3,\ldots,N$.

If the feeds are located closely, the main lobe will be enhanced and extended. With a reasonable arrangement of the feed locations, the sidelobes will be partly counteracted, for the odd and even sidelobes are just the opposite in sign. Moreover, the extended main lobe achieves a wider swath and finer azimuth resolution.

Fig. 7 shows the pattern that uses 4 × 2 feeds, 3.9 m dia., and 2.48 m focal length reflector. There are four feeds in the elevation at an interval of 2.07 cm and two feeds in the azimuth at an interval of 2.26 cm. As shown in Fig. 7(c), the sidelobes of the sum beam are much lower than the original one. The azimuth beamwidth is about 0.58°, which corresponds to the 3 m azimuth resolution design. Moreover, the elevation angle spreads to 1.5°, which extends the range swath effectively.

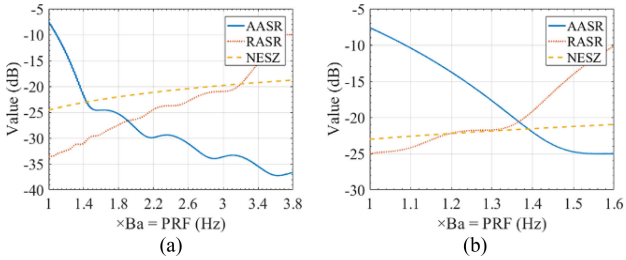

Fig. 8. Ambiguity of the multifeed reflector antenna. (a) Ambiguities and NESZ changing with PRF and 45° incidence and emergence angle. (b) Ambiguities and NESZ changing with PRF and 60° incidence and emergence angle.

Based on the proposed antenna pattern, the AASR, RASR, and the worst NESZ depending on PRF are updated and shown in Fig. 8. Comparing with Fig. 5(b), with the same observation angle, Fig. 8(a) has a better performance and the swath is extended to 20 km. Fig. 8(b) shows an extreme case in which the incidence angle and the emergence angle are both 60° and the swath is 40 km.

Since the azimuth ambiguity targets are better focused than the range ambiguity ones, AASR should be set lower than RASR. Thus, ConGalSAR selects 1.39 × azimuth bandwidth as the PRF, which approximately equal to 3880 Hz and the AASR is −22 dB, RASR is −20 dB, and the worst NESZ is −21.5 dB. The performance parameters mentioned above conform to most of the existing SAR systems.

IV. Resolution-Preserving Ambiguity Suppression Based on Amplitude-Modulated Chirps

According to (6), RASR is much more complex than AASR. Even though applying the proposed multifeed reflector antenna can effectively suppress the ambiguity, there will be the remnant of the ambiguity in the image caused by strong targets, which still impacts the interpretation severely.

As discussed in Section II, the characteristics of the azimuth and range ambiguities are quite different, especially for the weighting of the antenna patterns of the main and ambiguity areas. In [13] and [25], a spectral selection and extrapolation algorithm are proposed by us to suppress the azimuth ambiguity with better robustness and achieve a high-resolution and wide-swath observation. Inspired by this, a resolution-preserving range ambiguity suppression algorithm based on the amplitude-modulated chirps is proposed, in which the transmitting signal is artificially weighted to imitate the effect of the antenna pattern weighting in the azimuth. This method could suppress the residual range ambiguity more, especially for the large dynamic scenes.

The alternating amplitude-modulated chirps as the transmitting signals are described as

$$\begin{cases}S_{t1}(t)=w(t)\exp\left\{j\pi K_r t^2\right\}\\ S_{t2}(t)=w(t)\exp\left\{-j\pi K_r t^2\right\}\end{cases} \quad (14)$$

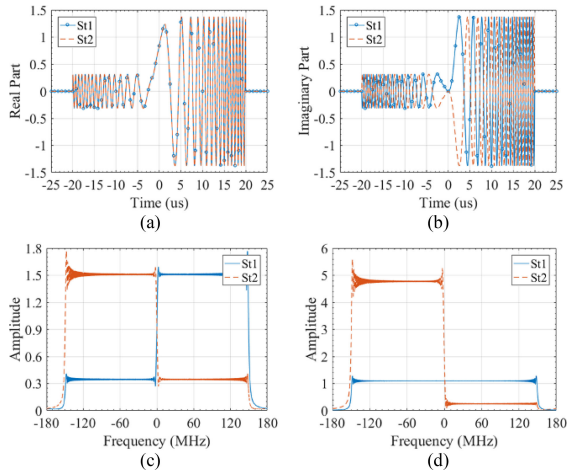

Fig. 9. Amplitude-modulated chirps with $a = 0.9$. (a) Real part of the alternating transmitting signals. (b) Imaginary part of the alternating transmitting signals. (c) Signals in the frequency domain. (d) Frequency compensating result for S_{t1}.

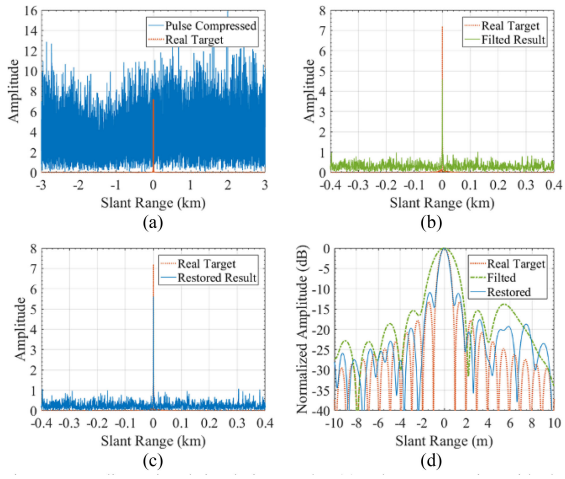

Fig. 10. 1-D simulation results. (a) Pulse compression with the phase compensation. (b) Bandpass filtering result. (c) Spectral extrapolating result. (d) Interpolation results.

where K_r is the chirp rate and $w(t)$ is the amplitude modulation function

$$w(t) = \text{rect}\left(\frac{4t + T_r}{2T_r}\right)\sqrt{1-a} + \text{rect}\left(\frac{4t - T_r}{2T_r}\right)\sqrt{1+a} \tag{15}$$

where T_r is the pulse width and $0 < a < 1$ is a modulation factor, which makes the transmitting power equal to the usual one.

The signals in the time domain and frequency domain are shown in Fig. 9(a)–(c), respectively. The echoes of different transmitting pulses have different frequency domain weights. As shown in Fig. 9(d), with the frequency compensation for S_{t1} (including both of phase and amplitude), the spectrum of the main zone [the area covered by the half-power beamwidth in the range shown in Fig. 3(b)] recovers to the chirp signal but with worse RASR. The signals can be separated by the frequency filter and the image after filtering has a lower RASR but lower resolution.

Through the frequency filtering, the pulse-compressed result can be separated into two parts with different RASR and lower resolution. The lower RASR part of the echo is from the main zone and the higher part is from the ambiguity zone [the area near the main zone shown in Fig. 3(b)], which can be filtered out by the bandpass filter. Then the key point is to restore the resolution robustly while keeping the lower RASR.

The spectral extrapolation algorithm proposed in [13] takes the high resolution and high azimuth ambiguity image as prior and reconstructs a high-resolution image from a narrow bandwidth and low ambiguity image robustly. Similarly, the algorithm can also be used in the range resolution recovery.

Supposed that one discrete signal along with the range after the frequency compensation is $\mathbf{x}_0$ [shown in Fig. 9(d)] and $\mathbf{F}$ is a Fourier transform matrix. The frequency-domain signal $\mathbf{y}_0$ is

$$\mathbf{y}_0 = \mathbf{F}\mathbf{x}_0. \tag{16}$$

With diagonal filtering matrix $\mathbf{L}$, the bandpass filtered result of $\mathbf{y}_0$ is

$$\mathbf{y} = \mathbf{L}\mathbf{y}_0 = \mathbf{L}\mathbf{F}\mathbf{x}_0 = \mathbf{A}\mathbf{x}_0. \tag{17}$$

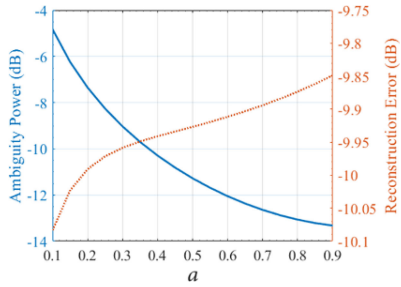

Fig. 11. Implications of modulation factor a. The curves just reflect the general trend of change because the specific values are closely related to the practical RASR, SNR, and the distribution characteristic of the scene.

The reconstructed result of $\mathbf{x}_0$ based on $\mathbf{y}$ is

$$\hat{\mathbf{x}} = \mathbf{W}\mathbf{A}^*(\mathbf{A}\mathbf{W}\mathbf{A}^*)^{-1}\mathbf{y} \tag{18}$$

where $\mathbf{W}$ is a diagonal matrix

$$\mathbf{W} = \begin{bmatrix} |\mathbf{x}_0[1]|^2 & 0 & \cdots & 0 \\ 0 & |\mathbf{x}_0[2]|^2 & \cdots & 0 \\ \vdots & \vdots & \ddots & \vdots \\ 0 & 0 & \cdots & |\mathbf{x}_0[N]|^2 \end{bmatrix}. \tag{19}$$

Considering Fig. 9(c) and (15), the ambiguity energy can be suppressed $(2-a)/a$ compared with the usual chirp signal after the bandpass filtering. However, the spectral extrapolation introduces a recovering noise into the image, which causes the suppression reducing to $\sqrt{(2-a)/a}$.

The processing results are shown in Fig. 10. There is one target at the center of the scene and the range ambiguity is so strong that it covers the real target after the pulse compression [Fig. 10(a)]. With the bandpass filtering, the ambiguity is suppressed and the real target appears [as shown in Fig. 10(b)]. However, the resolution goes worse [dashed dot line in Fig. 10(d)]. By the spectral extrapolation (18), the resolution is restored [see full line in Fig. 10(d)]. Meanwhile, the ambiguity is well suppressed [as shown in Fig. 10(c)].

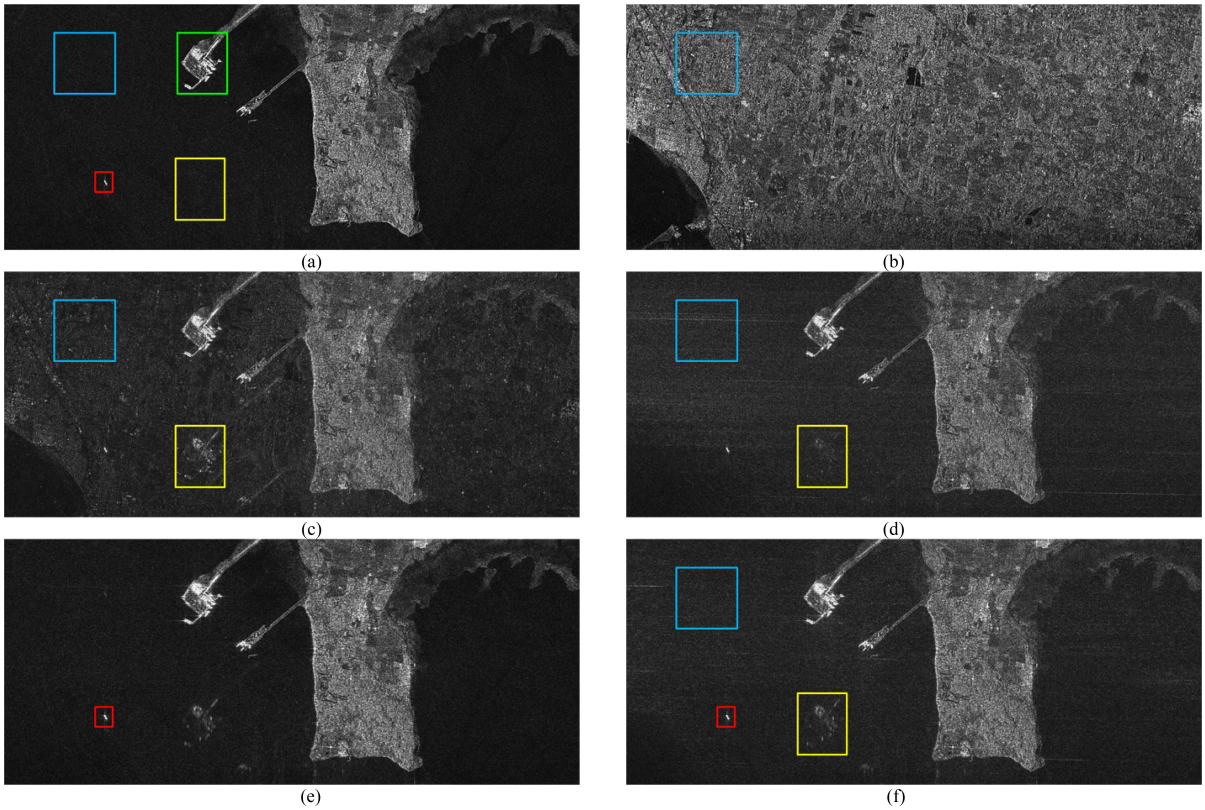

Fig. 12. Ambiguity suppression. (a) Original image is the Delta Port in Vancouver. (b) Range ambiguity source is the urban area in Vancouver. (c) Simulation result based on the one-way paraboloid reflector antenna, in which the ambiguity is very strong to be clearly seen. (d) Using the multifeed reflector antenna and up/down modulated chirps, the azimuth ambiguity is significantly suppressed, and the range ambiguity is scattered. (e) Range ambiguity suppression by the bandpass filtering. (f) Range resolution restoring by the spectral extrapolation algorithm.

The selection of modulation factor a is an important part of this method. With the increasing of a, the range ambiguity suppression becomes better; however, the robustness of the spectral extrapolation algorithm decreases (as shown in Fig. 11). An essential condition is that the power of the higher modulation part of the echo must be bigger than the power of the lower modulation part of the ambiguity. Otherwise, the real targets will still be covered by the ambiguity after the bandpass filtering and the spectral extrapolation algorithm will fail as well.

V. Experiments

In this section, we use the data obtained from Radarsat-1, which is proposed in [28] for simulation and experiments. The resolution of the image is about 10 m (mode: Fine Beam 2), the effective azimuth bandwidth and PRF are 970 Hz and 1257 Hz, respectively, the equivalent velocity is 7062 m/s, the distance between the radar and the center of the scene is 1000 km, and the transmitting pulse bandwidth is 30 MHz.

Delta Port is selected in this simulation and Fig. 12(a) shows the original scene. At the center of the image, there is a strong target on the sea [marked with a green box in Fig. 12(a)], which leads to a serious ambiguity along the azimuth [marked with a yellow box in Fig. 12(c)]. The urban area [see Fig. 12(b)] is the range ambiguity source, whose echoes are superimposed with one of the main zones together. With a one-way antenna pattern simulation, the image has the serious ambiguity interference [see Fig. 12(c)].

As shown in Fig. 12(d), using the multifeed reflector antenna proposed in Section III, the azimuth ambiguity is suppressed significantly (marked with a yellow box).

In order to evaluate the performance of the azimuth ambiguity suppression, the improvement of AASR is expressed as

$$\begin{aligned}\mathrm{AASR}_{\mathrm{improve}} &= 10\log_{10}\left(\frac{\bar{E}_p-\bar{E}_0}{\bar{E}_c}\right)-10\log_{10}\left(\frac{\bar{E}_m-\bar{E}_0}{\bar{E}_c}\right)\\ &= 10\log_{10}\left[\left(\bar{E}_p-\bar{E}_0\right)/\left(\bar{E}_m-\bar{E}_0\right)\right] \qquad (20)\end{aligned}$$

where $\bar{E}_c$ is the mean energy of the ambiguity source [green box in Fig. 12(a)], $\bar{E}_0$ is the mean energy of the background behind the ambiguity target in the original image [yellow box in Fig. 12(a)], $\bar{E}_p$ is the energy of the strong ambiguity target in the one-way paraboloid reflector antenna image [yellow box in Fig. 12(c)], and $\bar{E}_m$ is the energy of the strong ambiguity target in the multifeed reflector antenna image [yellow box in Fig. 12(f)].

The zooms of the targets in these images are shown in Fig. 13. The AASR goes from -14.0 to -26.8 dB and the improvement is about 12.8 dB, satisfying the ASR design of ConGalSAR. There is one point that should be concerned is that because the background energy is weaker than that in Fig. 12(d), the azimuth ambiguity in Fig. 12(e) looks clearer.

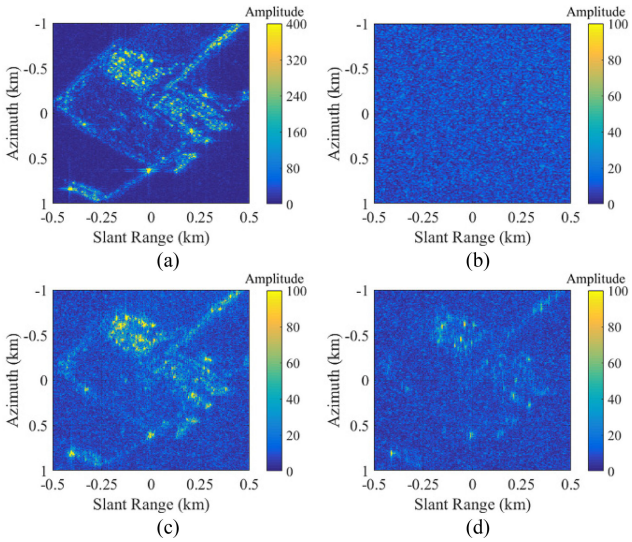

Fig. 13. Zooms of the port. (a) Azimuth ambiguity source in the green box of the original image in Fig. 11(a). (b) Background behind the ambiguity target in the yellow box of Fig. 11(a). (c) Ambiguity target with the one-way paraboloid reflector antenna in the yellow box of Fig. 11(c). (d) Ambiguity target with the multifeed reflector antenna in the yellow box of Fig. 11(f).

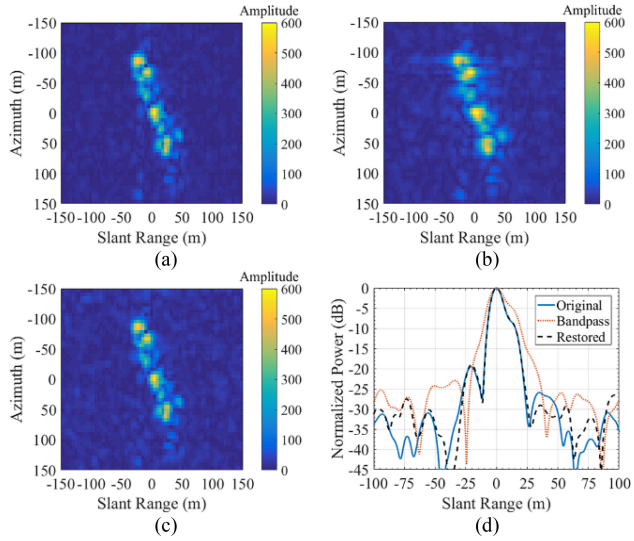

Fig. 14. Zooms of the ship. (a) Original image. (b) Bandpass filtering result. (c) Spectral extrapolation result. (d) Interpolation results of the strongest point on the ship.

For the range ambiguity, calculating the mean energy of the sea, the improvement of RASR is expressed as

$$\begin{aligned}\mathrm{RASR}_{\mathrm{improve}} &= 10\log_{10}\left(\frac{\bar{E}_u-\bar{E}_0}{\bar{E}_s}\right)-10\log_{10}\left(\frac{\bar{E}_e-\bar{E}_0}{\bar{E}_s}\right)\\ &= 10\log_{10}\left[\left(\bar{E}_u-\bar{E}_0\right)/\left(\bar{E}_e-\bar{E}_0\right)\right] \qquad (21)\end{aligned}$$

where $\bar{E}_s$ is the mean energy in the range ambiguity source image [blue box in Fig. 12(b)], $\bar{E}_0$ is the mean energy of the background behind the ambiguity target in the original image [blue box in Fig. 12(a)], $\bar{E}_u$ is the mean energy in the one-way paraboloid reflector antenna image [see Fig. 12(c)], and $\bar{E}_e$ is the mean energy in the up and down chirp modulation and proposed multifeed reflector antenna image [blue box in Fig. 12(d)]. The RASR goes from -17.0 to -20.1 dB.

With the up and down modulation chirps proposed in Section IV, the false target is defocused; however, the range ambiguity energy still remains in the image [see Fig. 12(d)].

Processing with the proposed amplitude-modulated chirps, the range ambiguity is suppressed significantly [as shown in Fig. 12(e)] compared with Fig. 12(d), with the improvement of RASR of about 4.73 dB [$\bar{E}_e$ is calculated with the blue box in Fig. 12(f) and $\bar{E}_u$ is calculated with the blue box in Fig. 12(d)]. Then, Fig. 12(f) shows the resolution restored results with the spectral extrapolation algorithm.

The ships [marked with the red boxes in Fig. 12(a), (e), and (f)] are zoomed for reflecting the resolution maintenance. As shown in Fig. 14(c), the ship has not changed significantly compared with the original image [see Fig. 14(a)]. Fig. 14(d) shows the range slices of the strongest point on the ship, which affirms that the resolution is restored well.

To sum up, the final result after the proposed comprehensive ambiguity suppression processing is greatly improved compared with the original ambiguous image in Fig. 11(c).

VI. Conclusion

A comprehensive method of the ambiguity suppression for ConGaLSAR is proposed in this article, solving the ASR deterioration caused by the special antenna pattern weighting in the system.

First, a multifeed reflector antenna is adopted in the hardware design to suppress the ambiguities and extend the range swath, which displaces the single-feed circle reflector antenna. Through the reasonable arrangement of the multifeed locations, the sidelobes are partly counteracted, while the extended main lobe achieves better swath and resolution. With the digital simulation, the AASR is improved from -14 -26.8 dB with an improvement of 12.8 dB, while the RASR is improved from -17.0 to -20.1 dB, restoring to the ASR system design of -20 dB and the range swath is extended to 40 km at the best case.

Afterward, a resolution preserving range ambiguity suppression algorithm based on the amplitude-modulated chirps is proposed to suppress the range ambiguity more aiming at the large dynamic scenes. The illuminator transmits the quasi-orthogonal signals alternatingly, which are constructed as the amplitude-modulated chirps. By the bandpass filtering in each receiving window, RASR is improved about 4.73 dB more, while the resolution loss is well restored by the spectral extrapolation.

Simulating with the Radarsat-1 echo data, the proposed comprehensive method is proved to be more effective for the ambiguity suppression in ConGaLSAR, which also provides an essential reference in the engineering application in the future.

References

[1] P. Xiao, B. Liu, and W. Guo, "ConGaLSAR: A constellation of geostationary and low earth orbit synthetic aperture radar," *IEEE Geosci. Remote Sens. Lett.*, to be published, doi: 10.1109/LGRS.2019.2962574.

[2] G. Krieger *et al.*, "MirrorSAR: A fractionated space radar for bistatic, multistatic and high-resolution wide-swath SAR imaging," in *Proc. IEEE Int. Geosci. Remote Sens. Symp.*, Fort Worth, TX, USA, Jul. 2017, pp. 149–152.

[3] G. Krieger, M. Zonno, J. Mittermayer, A. Moreira, S. Huber, and M. Rodriguez-Cassola, "MirrorSAR: A fractionated space transponder concept for the implementation of low-cost multistatic SAR missions," in *Proc. 12th Eur. Conf. Synthetic Aperture Radar*, Aachen, Germany, Jun. 2018, pp. 1359–1364.
[4] M. Zonno, G. Krieger, M. Rodriguez-Cassola, J. Mittermayer, and A. Moreira, "A MirrorSAR-based single-pass dual-baseline SAR interferometer for the generation of very high quality DEMs," in *Proc. 12th Eur. Conf. Synthetic Aperture Radar*, Aachen, Germany, Jun. 2018, pp. 1256–1261.
[5] J. C. Curlander and R. N. McDonough, *Synthetic Aperture Radar: Systems and Signal Processing*. Hoboken, NJ, USA: Wiley, 1991.
[6] J. Mittermayer and J. M. Martinez, "Analysis of range ambiguity suppression in SAR by up and down chirp modulation for point and distributed targets," in *Proc. IEEE Int. Geosci. Remote Sens. Symp.*, Jul. 2003, pp. 4077–4079.
[7] J. Akhtar, "Cancellation of range ambiguities with block coding techniques," in *Proc. IEEE Radar Conf.*, Pasadena, CA, USA, to be published, doi: 10.1109/RADAR.2009.4976978.
[8] V. Riché, S. Méric, J.-Y. Baudais, and É. Pottier, "Investigations on OFDM signal for range ambiguity suppression in SAR configuration," *IEEE Trans. Geosci. Remote Sens.*, vol. 52, no. 7, pp. 4194–4197, Jul. 2014.
[9] U. Stein and M. Younis, "Suppression of range ambiguities in synthetic aperture radar systems," in *Proc. IEEE Region 8 Eurocon*, Ljubljana, Slovenia, Sep. 2003, pp. 417–421.
[10] F. K. Li and W. T. K. Johnson, "Ambiguities in spacebornene synthetic aperture radar systems," *IEEE Trans. Aerosp. Electron. Syst.*, vol. AES-19, no. 3, pp. 389–397, May 1983.
[11] A. Moreira, "Suppressing the azimuth ambiguities in synthetic aperture radar images," *IEEE Trans. Geosci. Remote Sens.*, vol. 31, no. 4, pp. 885–894, Jul. 1993.
[12] A. M. Guarnieri, "Adaptive removal of azimuth ambiguities in SAR images," *IEEE Trans. Geosci. Remote Sens.*, vol. 43, no. 3, pp. 625–633, Mar. 2005.
[13] Y. Wu, Z. Yu, P. Xiao, and C. Li, "Suppression of azimuth ambiguities in spaceborne SAR images using spectral selection and extrapolation," *IEEE Trans. Geosci. Remote Sens.*, vol. 56, no. 10, pp. 6134–6147, Oct. 2018.
[14] M. Younis, C. Fischer, and W. Wiesbeck, "Digital beamforming in SAR systems," *IEEE Trans. Geosci. Remote Sens.*, vol. 41, no. 7, pp. 1735–1739, Jul. 2003.
[15] G. Krieger, N. Gebert, and A. Moreira, "Unambiguous SAR signal reconstruction from nonuniform displaced phase center sampling," *IEEE Geosci. Remote Sens. Lett.*, vol. 1, no. 4, pp. 260–264, Oct. 2004.
[16] F. Bordoni, M. Younis, E. M. Varona, and G. Krieger, "Adaptive scan-on-receive based on spatial spectral estimation for high-resolution, wide-swath synthetic aperture radar," in *Proc. IEEE Int. Geosci. Remote Sens. Symp.*, Cape Town, South Africa, Jul. 2009, pp. I-64–I-67.
[17] M. Villano, G. Krieger, and A. Moreira, "Staggered SAR: High-resolution wide-swath imaging by continuous PRI variation," *IEEE Trans. Geosci. Remote Sens.*, vol. 52, no. 7, pp. 4462–4479, Jul. 2014.
[18] C. Ma, X. Hu, T. S. Yeo, B. P. Ng, and Q. Zhang, "Matrix III-condition analysis in spectrum recovery of DPCA HRWS SAR imaging," *IEEE Geosci. Remote Sens. Lett.*, vol. 16, no. 1, pp. 55–59, Jan. 2019.
[19] D. Cerutti-Maori, I. Sikaneta, J. Klare, and C. H. Gierull, "MIMO SAR processing for multichannel high-resolution wide-swath radars," *IEEE Trans. Geosci. Remote Sens.*, vol. 52, no. 8, pp. 5034–5055, Aug. 2014.
[20] M. Younis, T. Rommel, F. Bordoni, G. Krieger, and A. Moreira, "On the pulse extension loss in digital beamforming SAR," *IEEE Geosci. Remote Sens. Lett.*, vol. 12, no. 7, pp. 1436–1440, Jul. 2015.
[21] M. I. Skolnik, *Introduction to Radar Systems*, 2nd ed. New York, NY, USA: McGraw-Hill, 1981.
[22] A. Moreira, P. Prats-Iraola, M. Younis, G. Krieger, I. Hajnsek, and K. P. Papathanassiou, "A tutorial on synthetic aperture radar," *IEEE Geosci. Remote Sens. Mag.*, vol. 1, no. 1, pp. 6–43, Mar. 2013.
[23] U. Naftaly and R. Levy-Nathansohn, "Overview of the TECSAR satellite hardware and mosaic mode," *IEEE Geosci. Remote Sens. Lett.*, vol. 5, no. 3, pp. 423–426, Jul. 2008.
[24] G. Krieger *et al.*, "The tandem-L mission proposal: Monitoring earth's dynamics with high-resolution SAR interferometry," in *Proc. IEEE Radar Conf.*, Pasadena, CA, USA, to be published, doi: 10.1109/RADAR.2009.4977077.
[25] P. Xiao, M. Liu, W. Guo, and J. Yu, "The range ambiguity suppression based on amplitude modulation chirp," in *Proc. IEEE Geosci. Remote Sens. Symp.*, Yokohama, Japan, Aug. 2019, pp. 688–691.
[26] L. C. Potter and K. S. Arun, "Energy concentration in band-limited extrapolation," *IEEE Trans. Acoust., Speech, Signal Process.*, vol. 37, no. 7, pp. 1027–1041, Jul. 1989.
[27] M. I. Skolnik, *Radar Handbook*, 3rd ed. New York, NY, USA: McGraw-Hill, 2008.
[28] I. G. Cumming and F. H.-C. Wong, *Digital Processing of Synthetic Aperture Radar Data: Algorithms and Implementation*. Norwood, MA, USA: Artech House, 2005.

Peng Xiao (Member, IEEE) was born in Harbin, Heilongjiang, China, in 1984. He received the B.S. degree in communication engineering and the Ph.D. degree in communication and information systems from the School of Electronic and Information Engineering, Beihang University, Beijing, China, in 2007 and 2014, respectively.

From 2014 to 2017, he held a Postdoctoral position with Beihang University, Beijing, China. Since 2017, he has been an Assistant Research Scientist with the Qian Xuesen Laboratory of Space Technology, China Academy of Space Technology, Beijing, China. His research interests include innovative remote sensing systems and applications based on ultrawide swath imaging with synthetic aperture radar systems, multistatic satellite formations, and the development of advanced signal algorithms.

Wei Guo was born in Xi'an, Shaanxi, China, in 1990. He received the B.S. degree in electronic and information engineering and the Ph.D. degree in signal and information processing from the School of Electronic and Information Engineering, Beihang University, Beijing, China, in 2012 and 2018, respectively.

From September 2016 to February 2017, he was a Visiting Research Student with the Centre for Terrestrial Carbon Dynamics, University of Sheffield, Sheffield, U.K. From November 2018 to December 2018, he was a Visiting Scholar with the Qian Xuesen Laboratory of Space Technology, China Academy of Space Technology, Beijing, China. Since February 2019, he has been a Research Assistant with the Department of Land Surveying and Geo-Informatics, The Hong Kong Polytechnic University, Kowloon, Hong Kong. His research interests include ionosphere exploration, compensation of ionospheric effects on SAR systems, long wavelength SAR signal processing, polarimetric calibration, and tomography.

Youming Wu was born in Nanchang, Jiangxi, China, in 1990. He received the B.S. degree in electronics engineering and the Ph.D. degree in signal and information processing from Beihang University, Beijing, China, in 2013 and 2020, respectively.

He is currently an Assistant Professor with the Aerospace Information Research Institute, Chinese Academy of Sciences, Beijing, China. His research interests include signal processing for wide-swath SAR and the improvement of spaceborne SAR image quality.

Bo Liu received the Ph.D. degree in signal and information processing from the Institute of Electronics, Chinese Academy of Sciences, Beijing, China, in 2013.

Since 2013, he has been a Research Assistant with the Qian Xuesen Laboratory of Space Technology, China Academy of Space Technology, Beijing, China. His research interests include space-based radar system design, moving target imaging detection, and intelligent radar systems and algorithms.